Earthq Eng & Eng Vib (2021) 20: 887-904 **DOI**: https://doi.org/10.1007/s11803-021-2060-5

Longitudinal integral response deformation method for the seismic analysis of a tunnel structure

Liu Jingbo†, Wang Dongyang‡ and Bao Xin‡

Department of Civil Engineering, Tsinghua University, Beijing 100084, China

Abstract: For the longitudinal seismic response analysis of a tunnel structure under asynchronous earthquake excitations, a longitudinal integral response deformation method classified as a practical approach is proposed in this paper. The determinations of the structural critical moments when maximal deformations and internal forces in the longitudinal direction occur are deduced as well. When applying the proposed method, the static analysis of the free-field computation model subjected to the least favorable free-field deformation at the tunnel buried depth is performed first to calculate the equivalent input seismic loads. Then, the equivalent input seismic loads are imposed on the integral tunnel-foundation computation model to conduct the static calculation. Afterwards, the critical longitudinal seismic responses of the tunnel are obtained. The applicability of the new method is verified by comparing the seismic responses of a shield tunnel structure in Beijing, determined by the proposed procedure and by a dynamic time-history analysis under a series of obliquely incident out-of-plane and in-plane waves. The results show that the proposed method has a clear concept with high accuracy and simple progress. Meanwhile, this method provides a feasible way to determine the critical moments of the longitudinal seismic responses of a tunnel structure. Therefore, the proposed method can be effectively applied to analyze the seismic response of a long-line underground structure subjected to non-uniform excitations.

Keywords: underground tunnel; longitudinal integral response deformation method; asynchronous seismic excitation; critical moment

1 Introduction

To study the seismic performance of underground structures subjected to non-uniform excitations, researchers in recent years have conducted a series of shaking table tests (Jiang *et al*., 2010; Li *et al*., 2015; Gu *et al*., 2017; Yu *et al*., 2018). However, limited by practical conditions such as bearing capacities and simulations of dynamic boundaries, the experimental results cannot accurately reflect the distributions of internal structural forces, and the tests of the large-scale modules can be hardly conducted. Consequently, it is necessary to establish some numerical simulation methods to analyze the seismic responses of underground structures subjected to asynchronous earthquake inputs.

Current analysis methods for the seismic responses of underground structures could be broadly separated into two categories following their mechanical characteristics: the dynamic time-history method (Fu *et al*., 2016) and the practical method (Liu and Shi, 2006; Liu *et al*., 2013a; Xu *et al*., 2017). More specifically, the free-field deformation method, the flexibility coefficient method, the response displacement method, the response acceleration method (Tateishi, 2005) and the pushover method (Liu *et al*., 2014) all belong to the category of practical techniques. Although the dynamic time-history method has high computational precision, it has been applied inconveniently in the aseismic designs of actual projects due to extreme computational demands. In addition, the rigorous implementations of artificial boundaries and seismic wave inputs in the dynamic time-history analysis also present difficulties for engineers, especially when performing the seismic analysis of a three-dimensional soil-structure interaction system. By comparison, practical methods that require simpler analysis models and a lesser workload have a wider range of applications in the aseismic designs of underground constructions. For instance, two types of integral response deformation methods have been put forward, which are applicable for the lateral aseismic analysis of underground structures with either regular shapes or arbitrary shapes (Liu *et al*., 2013b, 2014). These two practical methods take into consideration the soil-structure interactions directly through building the integral soil-structure computing models and avoid the extra computation costs and errors brought by the coefficients of foundation springs established in the

Correspondence to: Wang Dongyang, Department of Civil Engineering, Tsinghua University, Beijing 100084, China
Tel: +86-13811499702
E-mail: dongyangw@126.com
†Professor; ‡PhD

Supported by: National Natural Science Foundation of China under Grant No. 51478247
Received September 13, 2018; **Accepted** May 30, 2019

traditional response displacement method. Additionally, when dealing with complex structural cross sections, the calculation progress of the equivalent input seismic loads using the integral response deformation method is identically convenient.

Currently, as metro systems throughout China are under a massive construction phase, the seismic behavior of underground tunnels has become an essential research topic in the earthquake engineering field. Unlike the conventional underground structures, the seismic performance of a tunnel structure with a large longitudinal-scale would be significantly affected by spatial variations in ground motions. Hence, the magnitudes of structural deformations and internal forces in the longitudinal direction can no longer be ignored. Unfortunately, there is little research focusing on analysis methods in terms of the longitudinal seismic performance of a tunnel structure compared to abundant achievements in the lateral direction. Additionally, there are no adequate suggestions provided in domestic professional codes. Only the free-field deformation method (John and Zahrah, 1987) and the response displacement method (Shao and Lei, 2013), employed by the "Code for Seismic Design of Nuclear Power Plants" (GB 50267-97, China Planning Press, Beijing) and the "Code for Seismic Design of Urban Rail Transit Structures" (GB 50909-2014, China Planning Press, Beijing) have typically been applied for the longitudinal seismic analysis of a tunnel structure.

However, there are several technical shortcomings of the practical methods recommended by the two current codes mentioned above. The free-field deformation method does not consider soil-structure interaction under earthquake inputs. This method assumes that the deformation of an underground structure is completely controlled by the movements of its surrounding soil, which means that the construction of the underground structure introduces no influence on the seismic response of the soil medium. Thus, the free-field deformation method is only suitable for the aseismic design of underground pipelines and tunnels with small cross-sectional areas, whereas it is more reasonable that the response displacement method is capable of considering the soil-structure interaction to some extent. Specifically, the response displacement method for the longitudinal seismic analysis of a tunnel structure builds a beam model to simulate the long-line tunnel structure and sets up discrete springs along the longitudinal structural axis to simulate the surrounding foundation soil. Equivalent input seismic loads, acting at the ends of the foundation springs away from the tunnel, are precisely the displacements of the soil medium relative to the embedded position of tunnel. During the implementation process of this response displacement method, the stiffness factors of those foundation springs can be calculated by using either empirical formulas or the static finite element analysis method. Equivalent input seismic loads are typically modeled as a sinusoidal wave-shape in the longitudinal direction or achieved by completing the dynamic analysis of the free wave field (He *et al*., 2017). In view of the operation process, the disadvantages of the response displacement method can be summarized in three aspects. First, the dispersive-layout springs cannot reflect the dynamic interactions of the continuous soil medium itself. Second, the stiffness factors of the foundation springs are calculated through different forms, which may result in a significant computational discrepancy of structural seismic responses. Third, the presumption of a sinusoidal-shape is not the actual distribution of the equivalent input seismic loads under asynchronous excitations.

To solve the problems existing in the longitudinal seismic analysis of an underground tunnel structure subjected to asynchronous seismic excitations, this paper proposes a longitudinal integral response deformation method. First, we start the discussion by establishing the basic procedure and calculation models of the proposed method. Then, the specific implementation of the proposed method is recommended, with an emphasis on the calculation of the free wave field and a determination of the critical moments of the structural longitudinal responses under asynchronous seismic excitations, such as out-of-plane (SH) and in-plane (SV and P) waves. As a result, the equivalent input seismic loads are obtained, and a static analysis of the integral soil-tunnel computing model can be performed. Lastly, taking a shield tunnel construction in Beijing as the three-dimensional research object, the validity and accuracy of the proposed method are verified by comparing the computational results with the accurate dynamic time-history solutions under a series of obliquely incident seismic waves, namely, SH and SV waves. It is revealed that the proposed method has conceptual simplicity and computational attractiveness. Meanwhile, this method provides a feasible idea of determining the critical moments for the longitudinal seismic responses of a tunnel structure under non-uniform excitations.

2 Methodology of the longitudinal integral response deformation method

As shown in Fig. 1(a), an underground tunnel is embedded in the layered half-space foundation. Interface S, denoted by the red color, is the exterior surface of the tunnel structure, namely, the contact surface between the tunnel and its surrounding soil. To analyze the longitudinal responses of the tunnel subjected to earthquakes, the proposed method requires both the relevant free-field finite element model and the integral soil-tunnel finite element model. Figure 1(b) shows the relevant three-dimensional free-field finite element model of the layered half-space foundation. The red zone enclosed by the interface S is filled with the same soil medium as the foundation-tunnel model in Fig. 1(a). For simplicity, only the cross-sectional mesh generation is illustrated

in the figures. Figure 1(c) shows the three-dimensional integral finite element model of the foundation-tunnel system. All the truncation boundaries of the two finite element models are completely constrained.

In view of the numerical models shown in Fig. 1 and the work of Liu *et al*. (2013b, 2014), the basic steps of the proposed method can be summarized as described below.

(1) Solve the three-dimensional free wave field. In the elastic half-space, the analytical solutions to the free wave field can be obtained. For the layered half-space, more considerations regarding the incident angles of the earthquake wave are required. If the seismic wave is vertically incident, the free wave field can be generally determined by equivalent linearization programs such as SHAKE91 (Idriss and Sun, 1992) and EERA (Bardet *et al*., 2000). Otherwise, for the obliquely incident wave, the free wave field can be calculated through analytical methods in the frequency domain (Knopoff, 1964; Wolf and Obernhuber, 1982a, 1982b). Moreover, the one-dimensional time-domain algorithm can be used to calculate the nodal movements of a vertical column in the free-field finite element model. Then, the three-dimensional free wave field can be acquired with a geometrical expansion in the layered half-space, in accordance with the propagation characteristics of the traveling waves (Liu and Wang, 2006; Liu and Wang, 2007; Zhao *et al*., 2013). Notably, for the in-plane wave incidence, a three-dimensional free wave field can be obtained through the use of the one-dimensional analytical method. There is no need to adopt the two-dimensional or three-dimensional analysis methods.

(2) Determine the critical moment of the longitudinal seismic response of the underground tunnel, which is the key procedure for converting the structural dynamic analysis into an equivalent static problem. In the lateral seismic analysis of an underground structure, the critical moment is exactly when the relative displacement between the structural top and bottom slabs reaches its peak value. However, for the longitudinal seismic analysis of underground long-line structure subjected to non-uniform earthquake inputs, determining the critical moment becomes a more complicated problem to be solved. Further details can be found in the following section.

(3) Calculate the equivalent input seismic loads. The seismic response of a three-dimensional free field at the critical moment can be confirmed after following the steps listed above. Hence, we achieve both the relevant free-field nodal displacements on the interface S and the free-field nodal accelerations of the soil-medium elements enclosed by the interface S at the critical moment. Apply these free-field displacements on the interface S nodes of the free-field finite element model in Fig. 1(b). Meanwhile, impose these free-field accelerations on the soil-medium-element nodes enclosed by the interface S of the same simulation model. Then, complete the static analysis to acquire a set of nodal reaction forces on the interface S at the critical moment. As a result, the equivalent input seismic loads of the proposed method are brought to light.

(4) Accomplish the static analysis of the integral soil-tunnel computation model. The equivalent input seismic loads acquired by the last step should be exerted on the interface S nodes of the integral soil-tunnel finite element model shown in Fig. 1(c). Then, the longitudinal maximal seismic response of the tunnel structure can be gained after performing the static analysis.

As seen from the general procedure and computing models clarified above, the longitudinal integral response deformation method is suitable for analyzing the critical seismic responses of underground tunnels subjected to various earthquake motions. The proposed method takes into consideration the soil-tunnel interaction directly through building the integral computation model, thus avoiding the extra workload and calculation error brought by the foundation springs of the classical response displacement method. Moreover, there are no limitations on the structural shapes enclosed by the interface S. Hence the new method described herein can be applied to more general problems, such as the longitudinal seismic response analysis of a tunnel structure with a large dimension or a variable cross section.

3 Implementation of the longitudinal integral response deformation method under SH waves

In this section the specific implementation of the proposed method under SH waves is represented. For

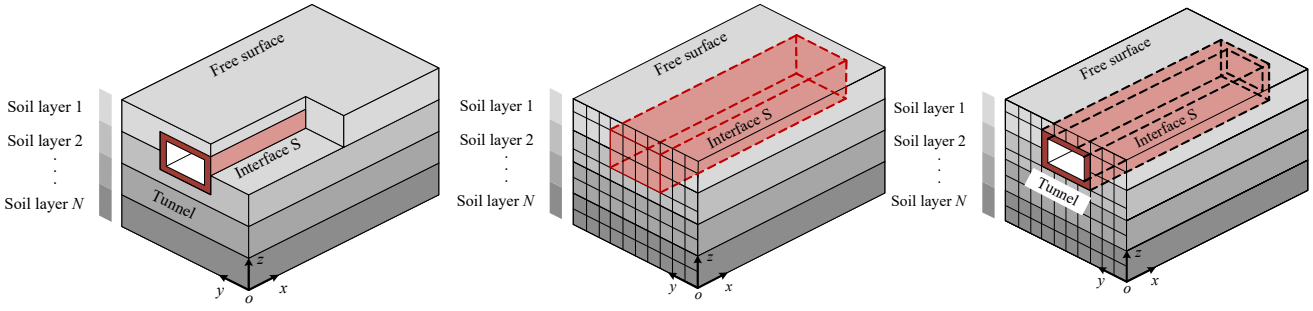

(a) Foundation-tunnel model (b) Free-field finite element model (c) Integral soil-tunnel finite element model

Fig. 1 Numerical model of the longitudinal integral response deformation method

brevity, the semi-infinite foundation is modeled as the elastic half-space.

3.1 Free-field seismic response

Figure 2 shows the elastic half-space model, where the x-axis and y-axis denote the two horizontal directions, and the z-axis denotes the vertical direction of the Cartesian coordinate system. The incident SH wave comes obliquely from the far field into the calculation zone. The angle between the z-axis and the incident SH wave direction is written as θ. The angle between the x-axis and the horizontal projection of the incident SH wave is designated as ϕ.

The displacement vector of the incident SH wave is written as $\boldsymbol{u}_{\mathrm{i}}^{\mathrm{SH}}(t)$. According to the wave propagation laws in the elastic half-space, the free-field displacement solution, written as $\boldsymbol{u}^0(x,y,z,t)$, is the summation of the incident-wave and reflected-wave displacement fields. For the oblique incidence of the SH wave, there is no conversion of wave forms. Therefore, the free-field displacement solution $\boldsymbol{u}^0(x,y,z,t)$ is composed of the incident SH wave and the reflected SH wave from the free surface, shown as Eq. (1):

$$\boldsymbol{u}^0(x,y,z,t)=\boldsymbol{u}_{\mathrm{i}}^{\mathrm{SH}}\left(t-\frac{x\sin\theta\cos\phi}{c_{\mathrm{S}}}-\frac{y\sin\theta\sin\phi}{c_{\mathrm{S}}}-\frac{z\cos\theta}{c_{\mathrm{S}}}\right)+\boldsymbol{u}_{\mathrm{r}}^{\mathrm{SH}}\left(t-\frac{x\sin\theta\cos\phi}{c_{\mathrm{S}}}-\frac{y\sin\theta\sin\phi}{c_{\mathrm{S}}}+\frac{z\cos\theta}{c_{\mathrm{S}}}\right) \tag{1}$$

where $\boldsymbol{u}^0(x,y,z,t)$ includes two displacement components in the x-axis and y-axis directions, written as $u_x^0(x,y,z,t)$ and $u_y^0(x,y,z,t)$, respectively; $\boldsymbol{u}_{\mathrm{r}}^{\mathrm{SH}}(t)$ is the displacement vector of the reflected SH wave; and c_{S} is the velocity of the shear wave in the elastic half-space.

Equation (1) leads to the following expression:

$$\begin{cases}\boldsymbol{u}^0(x,y,z,t)=\boldsymbol{u}^0\left(0,y,z,t-\dfrac{x}{c_x}\right)\\ c_x=\dfrac{c_{\mathrm{S}}}{\sin\theta\cos\phi}\end{cases} \tag{2}$$

where c_x is the apparent wave velocity in the x-axis direction.

Then, a relationship can be drawn between the high-order partial derivatives of $\boldsymbol{u}^0(x,y,z,t)$ with respect to the spatial variable x, and those with respect to the time variable t:

$$\frac{\partial^n\boldsymbol{u}^0(x,y,z,t)}{\partial x^n}=\left(-\frac{1}{c_x}\right)^n\frac{\partial^n\boldsymbol{u}^0(x,y,z,t)}{\partial t^n}\qquad n=1,\ 2,\ 3,\ \cdots \tag{3}$$

For any component of $\boldsymbol{u}^0(x,y,z,t)$, Eq. (3) is still valid. It can be proven that Eqs. (2) and (3) also work for elastic layered half-space issues.

3.2 Critical moment

As shown in Fig. 3, there is an underground tunnel embedded in the elastic half-space. The incident angles of the SH wave are still written as θ and ϕ. The horizontal and vertical coordinates of the tunnel centerline are y_{T} and z_{T}, respectively. The relevant free-field displacement time-history at the position of the tunnel centerline is written as $\boldsymbol{u}^0(x,y_{\mathrm{T}},z_{\mathrm{T}},t)$.

If the long-line tunnel has a relatively small cross-section dimension, it can be reasonably modeled as a constant-section beam embedded in the soil layer. The moving status of the tunnel can be quantified by the displacement vector of the structural centerline, written as $\boldsymbol{u}(x,y_{\mathrm{T}},z_{\mathrm{T}},t)$, including the components of the axial displacement $u_x(x,y_{\mathrm{T}},z_{\mathrm{T}},t)$ and the lateral displacement $u_y(x,y_{\mathrm{T}},z_{\mathrm{T}},t)$. Its force status can be measured by the axial force $N_x(x,y_{\mathrm{T}},z_{\mathrm{T}},t)$, the bending moment $M_z(x,y_{\mathrm{T}},z_{\mathrm{T}},t)$ and the shear force $V_y(x,y_{\mathrm{T}},z_{\mathrm{T}},t)$. Then, we can have the following equations through the bending theory of a beam:

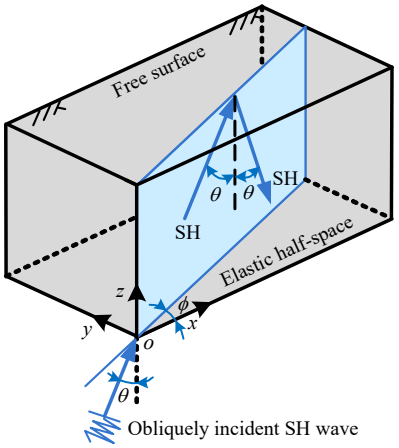

Fig. 2 Incidence and reflection of the SH wave on the ground surface in the elastic half-space

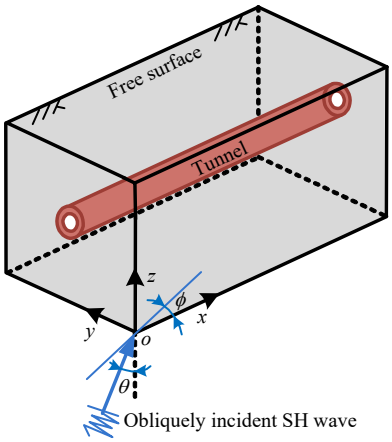

Fig. 3 A tunnel structure embedded in the elastic half-space

$$N_x\left(x,y_{\mathrm{T}},z_{\mathrm{T}},t\right)=EA\frac{\partial u_x\left(x,y_{\mathrm{T}},z_{\mathrm{T}},t\right)}{\partial x} \tag{4}$$

$$M_z\left(x,y_{\mathrm{T}},z_{\mathrm{T}},t\right)=-EI\frac{\partial^2 u_y\left(x,y_{\mathrm{T}},z_{\mathrm{T}},t\right)}{\partial x^2} \tag{5}$$

$$V_y\left(x,y_{\mathrm{T}},z_{\mathrm{T}},t\right)=-EI\frac{\partial^3 u_y\left(x,y_{\mathrm{T}},z_{\mathrm{T}},t\right)}{\partial x^3} \tag{6}$$

where EA, EI are the tensile stiffness and bending stiffness of the beam, respectively.

Considering the fact that the deformation of an underground structure is mainly controlled by its surrounding soil medium subjected to earthquake motions, we have:

$$\boldsymbol{u}\left(x,y_{\mathrm{T}},z_{\mathrm{T}},t\right)\propto\boldsymbol{u}^0\left(x,y_{\mathrm{T}},z_{\mathrm{T}},t\right) \tag{7}$$

$$N_x\left(x,y_{\mathrm{T}},z_{\mathrm{T}},t\right)\propto EA\frac{\partial u_x^0\left(x,y_{\mathrm{T}},z_{\mathrm{T}},t\right)}{\partial x} \tag{8}$$

$$M_z\left(x,y_{\mathrm{T}},z_{\mathrm{T}},t\right)\propto\left(-EI\right)\frac{\partial^2 u_y^0\left(x,y_{\mathrm{T}},z_{\mathrm{T}},t\right)}{\partial x^2} \tag{9}$$

$$V_y\left(x,y_{\mathrm{T}},z_{\mathrm{T}},t\right)\propto\left(-EI\right)\frac{\partial^3 u_y^0\left(x,y_{\mathrm{T}},z_{\mathrm{T}},t\right)}{\partial x^3} \tag{10}$$

where $u_x^0\left(x,y_{\mathrm{T}},z_{\mathrm{T}},t\right)$, $u_y^0\left(x,y_{\mathrm{T}},z_{\mathrm{T}},t\right)$ are the free-field axial and lateral displacements, respectively, corresponding to the embedded position of the tunnel structure.

Substituting Eq. (3) into Eqs. (8)–(10) in sequence results in:

$$N_x\left(x,y_{\mathrm{T}},z_{\mathrm{T}},t\right)\propto EA\left(-\frac{1}{c_x}\right)\frac{\partial u_x^0\left(x,y_{\mathrm{T}},z_{\mathrm{T}},t\right)}{\partial t} \tag{11}$$

$$M_z\left(x,y_{\mathrm{T}},z_{\mathrm{T}},t\right)\propto\left(-EI\right)\left(-\frac{1}{c_x}\right)^2\frac{\partial^2 u_y^0\left(x,y_{\mathrm{T}},z_{\mathrm{T}},t\right)}{\partial t^2} \tag{12}$$

$$V_y\left(x,y_{\mathrm{T}},z_{\mathrm{T}},t\right)\propto\left(-EI\right)\left(-\frac{1}{c_x}\right)^3\frac{\partial^3 u_y^0\left(x,y_{\mathrm{T}},z_{\mathrm{T}},t\right)}{\partial t^3} \tag{13}$$

Accordingly, we have:

$$\left|\boldsymbol{u}\left(x,y_{\mathrm{T}},z_{\mathrm{T}},t\right)\right|_{\max}\propto\left|\boldsymbol{u}^0\left(x,y_{\mathrm{T}},z_{\mathrm{T}},t\right)\right|_{\max} \tag{14}$$

$$\left|N_x\left(x,y_{\mathrm{T}},z_{\mathrm{T}},t\right)\right|_{\max}\propto\left|EA\frac{\partial u_x^0\left(x,y_{\mathrm{T}},z_{\mathrm{T}},t\right)}{\partial t}\right|_{\max} \tag{15}$$

$$\left|M_z\left(x,y_{\mathrm{T}},z_{\mathrm{T}},t\right)\right|_{\max}\propto\left|EI\frac{\partial^2 u_y^0\left(x,y_{\mathrm{T}},z_{\mathrm{T}},t\right)}{\partial t^2}\right|_{\max} \tag{16}$$

$$\left|V_y\left(x,y_{\mathrm{T}},z_{\mathrm{T}},t\right)\right|_{\max}\propto\left|EI\frac{\partial^3 u_y^0\left(x,y_{\mathrm{T}},z_{\mathrm{T}},t\right)}{\partial t^3}\right|_{\max} \tag{17}$$

As seen from Eqs. (14)–(17), the critical moments of structural longitudinal seismic responses are determined through the relevant free-field motions. For an arbitrary point on the tunnel structure subjected to obliquely incident SH waves, the critical moment of its displacement is specifically when the relevant free-field displacement in the same direction reaches the maximum. The critical moment of its axial force is when the relevant free-field axial velocity reaches the maximum. The critical moment of its bending moment is when the relevant free-field lateral acceleration reaches the maximum. The critical moment of its shear force is when the third order derivative of relevant free-field lateral displacement with respect to the time variable t reaches the maximum.

Hence, the critical moments of deformation and internal forces for any position of the tunnel structure are only related to the time-histories of free-field movements at the same location. This technique for confirming the longitudinal critical moments is quite different from that applied to the lateral seismic analysis of an underground structure.

3.3 Equivalent input seismic load

To calculate the equivalent input seismic loads of the proposed method, the free-field finite element model depicted in Fig. 1(b) should be built. Then, the critical free-field displacements corresponding to different physical quantities are applied on the Interface S nodes of the free-field finite element model. Nodal reaction forces on the Interface S can be obtained through static computations. In this way, the equivalent input seismic loads in correspondence to different physical quantities are ascertained.

Notably, the inertia force of the free field enclosed by the interface S does not count toward the calculation of equivalent input seismic loads because the structural response induced by this part of inertial force makes up a rather small percentage of the overall seismic response of the underground structure with a minor scale cross-section (Liu *et al*., 2014). Especially for a small cross-sectional tunnel simulated by the beam elements, the

contribution of the inertial force is so limited that, for simplicity, it can be considered negligible. However, if the tunnel has a large-scale cross-section that cannot be modeled as the beam element the influence of the inertial force should be taken into consideration.

3.4 Longitudinal seismic analysis of the tunnel structure

The integral soil-tunnel finite element model is established and is shown as Fig. 1(c). The equivalent input seismic loads corresponding to the critical seismic responses of different physical quantities, acquired in the last step, are applied on the interface S of the integral model. Then, the critical seismic responses of the tunnel structure can be obtained through a series of static calculations. In general, the midpoint of the computational model is chosen as a reference to observe the critical seismic responses. Such a treatment can avoid the impacts made by the boundary effects of structural ends, making the calculation results more convincing (Li, 2013).

4 Implementation of the longitudinal integral response deformation method under SV and P waves

In this section, the specific implementations of the proposed method under SV and P waves are represented. Unlike obliquely incident SH waves, the conversion of wave forms on the free surface may exist in this situation. The reflected waves from the free surface are composed of SV and P waves. According to the basic principle of the proposed method, we begin the discussions with the calculations of free-field seismic responses under obliquely incident SV and P waves, respectively. The semi-infinite foundation is still simplified as the elastic half-space.

4.1 Free-field seismic response

In Fig. 4, subfigures (a) and (b) show the incidences and reflections of the SV and P waves on the ground surface, respectively. The SV or P wave is obliquely incident from the far field into the calculation zone. The incident angles of the in-plane waves, θ and ϕ, have the same definitions as the SH wave incidence depicted in Fig. 2. The subscripts S and P stand for the SV and P waves, respectively. Subscripts 1 and 2 represent the incident conditions of SV and P waves, respectively.

4.1.1 Obliquely incident SV wave

In Fig. 4(a), the displacement vector of the incident SV wave is written as $\boldsymbol{u}_{\mathrm{i1}}^{\mathrm{SV}}(t)$. According to the wave propagation characteristics in the elastic half-space, the free wave field solution $\boldsymbol{u}^0(x,y,z,t)$ is the summation of the displacement fields of the incident SV wave, and the reflected SV and P waves, as shown in Eq. (18).

$$\begin{aligned}\boldsymbol{u}^0(x,y,z,t)=&\\ &\boldsymbol{u}_{\mathrm{i1}}^{\mathrm{SV}}\left(t-\frac{x\sin\theta_{\mathrm{S1}}\cos\phi}{c_{\mathrm{S}}}-\frac{y\sin\theta_{\mathrm{S1}}\sin\phi}{c_{\mathrm{S}}}-\frac{z\cos\theta_{\mathrm{S1}}}{c_{\mathrm{S}}}\right)+\\ &\boldsymbol{u}_{\mathrm{r1}}^{\mathrm{SV}}\left(t-\frac{x\sin\theta_{\mathrm{S1}}\cos\phi}{c_{\mathrm{S}}}-\frac{y\sin\theta_{\mathrm{S1}}\sin\phi}{c_{\mathrm{S}}}+\frac{z\cos\theta_{\mathrm{S1}}}{c_{\mathrm{S}}}\right)+\\ &\boldsymbol{u}_{\mathrm{r1}}^{\mathrm{P}}\left(t-\frac{x\sin\theta_{\mathrm{P1}}\cos\phi}{c_{\mathrm{P}}}-\frac{y\sin\theta_{\mathrm{P1}}\sin\phi}{c_{\mathrm{P}}}+\frac{z\cos\theta_{\mathrm{P1}}}{c_{\mathrm{P}}}\right)\end{aligned}\tag{18}$$

where $\boldsymbol{u}^0(x,y,z,t)$ includes three displacement components in the x-axis, y-axis and z-axis directions, written as $u_x^0(x,y,z,t)$, $u_y^0(x,y,z,t)$ and $u_z^0(x,y,z,t)$, respectively; $\boldsymbol{u}_{\mathrm{r1}}^{\mathrm{SV}}(t)$ and $\boldsymbol{u}_{\mathrm{r1}}^{\mathrm{P}}(t)$ are the displacement vectors of the reflected SV and P waves, respectively; c_{S} and c_{P} are the velocities of shear and compression waves in the elastic half-space, respectively; and θ_{P1} is the reflected angle of the P wave.

The following expression can be given by referring to Snell′s law:

$$\frac{c_{\mathrm{S}}}{\sin\theta_{\mathrm{S1}}}=\frac{c_{\mathrm{P}}}{\sin\theta_{\mathrm{P1}}}\tag{19}$$

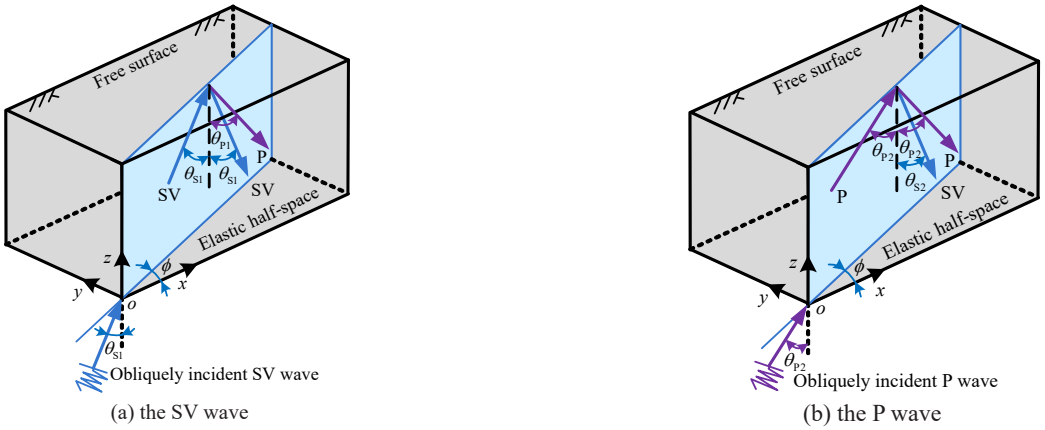

(a) the SV wave (b) the P wave

Fig. 4 Incidence and reflection of (a) the SV wave; (b) the P wave on the ground surface in the elastic half-space

Combining Eq. (18) with Eq. (19) provides the following expression:

$$\begin{cases} \boldsymbol{u}^0\left(x,y,z,t\right)=\boldsymbol{u}^0\left(0,y,z,t-\dfrac{x}{c_x}\right) \\ c_x=\dfrac{c_{\mathrm{S}}}{\sin\theta_{\mathrm{S1}}\cos\phi}=\dfrac{c_{\mathrm{P}}}{\sin\theta_{\mathrm{P1}}\cos\phi} \end{cases} \tag{20}$$

where c_x represents the apparent wave velocity in the *x*-axis direction.

Similarly, the relationship between the high-order partial derivatives of $\boldsymbol{u}^0\left(x,y,z,t\right)$ with respect to spatial variable *x* and those with respect to time variable *t* can be drawn as the following:

$$\begin{aligned} &\frac{\partial^n\boldsymbol{u}^0\left(x,y,z,t\right)}{\partial x^n}=\left(-\frac{1}{c_x}\right)^n\frac{\partial^n\boldsymbol{u}^0\left(x,y,z,t\right)}{\partial t^n} \\ &n=1,\ 2,\ 3,\ \cdots \end{aligned} \tag{21}$$

For any component of $\boldsymbol{u}^0\left(x,y,z,t\right)$, Eq. (21) is still rational. It can be proven that Eq. (20) and Eq. (21) are still applicable to the elastic layered half-space issues.

4.1.2 Obliquely incident P wave

In Fig. 4(b), the displacement vector of the incident P wave is denoted as $\boldsymbol{u}_{\mathrm{i2}}^{\mathrm{P}}\left(t\right)$. With reference to the wave propagation characteristics in the elastic half-space, the free wave field solution $\boldsymbol{u}^0\left(x,y,z,t\right)$ is the summation of the displacement fields of the incident P wave, and the reflected P and SV waves, as shown in Eq. (22).

$$\begin{aligned} &\boldsymbol{u}^0\left(x,y,z,t\right)= \\ &\boldsymbol{u}_{\mathrm{i2}}^{\mathrm{P}}\left(t-\frac{x\sin\theta_{\mathrm{P2}}\cos\phi}{c_{\mathrm{P}}}-\frac{y\sin\theta_{\mathrm{P2}}\sin\phi}{c_{\mathrm{P}}}-\frac{z\cos\theta_{\mathrm{P2}}}{c_{\mathrm{P}}}\right)+ \\ &\boldsymbol{u}_{\mathrm{r2}}^{\mathrm{P}}\left(t-\frac{x\sin\theta_{\mathrm{P2}}\cos\phi}{c_{\mathrm{P}}}-\frac{y\sin\theta_{\mathrm{P2}}\sin\phi}{c_{\mathrm{P}}}+\frac{z\cos\theta_{\mathrm{P2}}}{c_{\mathrm{P}}}\right)+ \\ &\boldsymbol{u}_{\mathrm{r2}}^{\mathrm{SV}}\left(t-\frac{x\sin\theta_{\mathrm{S2}}\cos\phi}{c_{\mathrm{S}}}-\frac{y\sin\theta_{\mathrm{S2}}\sin\phi}{c_{\mathrm{S}}}+\frac{z\cos\theta_{\mathrm{S2}}}{c_{\mathrm{S}}}\right) \end{aligned} \tag{22}$$

where $\boldsymbol{u}^0\left(x,y,z,t\right)$ includes three displacement components in the *x*-axis, *y*-axis and *z*-axis directions; $\boldsymbol{u}_{\mathrm{r2}}^{\mathrm{P}}\left(t\right)$ and $\boldsymbol{u}_{\mathrm{r2}}^{\mathrm{SV}}\left(t\right)$ are the displacement vectors of the reflected P and SV waves, respectively; and θ_{S2} is the reflected angle of the SV wave.

Next, the following expression, which is also applicable to the elastic layered half-space, can be given by referring to Eq. (22) and Snell′s law:

$$\begin{cases} \boldsymbol{u}^0\left(x,y,z,t\right)=\boldsymbol{u}^0\left(0,y,z,t-\dfrac{x}{c_x}\right) \\ c_x=\dfrac{c_{\mathrm{P}}}{\sin\theta_{\mathrm{P2}}\cos\phi}=\dfrac{c_{\mathrm{S}}}{\sin\theta_{\mathrm{S2}}\cos\phi} \end{cases} \tag{23}$$

where c_x is the apparent wave velocity in the *x*-axis direction.

Comparing Eq. (23) with Eq. (20), we draw the conclusion that Eq. (21) can also be derived under obliquely incident P waves.

Therefore, with the relationship shown in Eq. (21), we can make additional efforts to determine the critical moments of structural longitudinal seismic responses subjected to the in-plane waves.

4.2 Critical moment

At this time, the tunnel structure in Fig. 3 is subjected to obliquely incident in-plane waves. The displacement vector of the structural centerline can be still denoted as $\boldsymbol{u}\left(x,y_{\mathrm{T}},z_{\mathrm{T}},t\right)$, including the three components in the coordinate-axis directions, written as $u_x\left(x,y_{\mathrm{T}},z_{\mathrm{T}},t\right)$, $u_y\left(x,y_{\mathrm{T}},z_{\mathrm{T}},t\right)$ and $u_z\left(x,y_{\mathrm{T}},z_{\mathrm{T}},t\right)$. The structural force status is more complicated than the situation of suffering incident SH waves. More specifically, there are the axial force $N_x\left(x,y_{\mathrm{T}},z_{\mathrm{T}},t\right)$, the bending moments $M_y\left(x,y_{\mathrm{T}},z_{\mathrm{T}},t\right)$ and $M_z\left(x,y_{\mathrm{T}},z_{\mathrm{T}},t\right)$ around the *y*-axis and the *z*-axis, respectively, and the shear forces $V_y\left(x,y_{\mathrm{T}},z_{\mathrm{T}},t\right)$ and $V_z\left(x,y_{\mathrm{T}},z_{\mathrm{T}},t\right)$ along the *y*-axis and the *z*-axis directions, respectively. Then, we can obtain the following equations:

$$\boldsymbol{u}\left(x,y_{\mathrm{T}},z_{\mathrm{T}},t\right)\propto\boldsymbol{u}^0\left(x,y_{\mathrm{T}},z_{\mathrm{T}},t\right) \tag{24}$$

$$N_x\left(x,y_{\mathrm{T}},z_{\mathrm{T}},t\right)\propto EA\frac{\partial u_x^0\left(x,y_{\mathrm{T}},z_{\mathrm{T}},t\right)}{\partial x} \tag{25}$$

$$M_y\left(x,y_{\mathrm{T}},z_{\mathrm{T}},t\right)\propto\left(-EI\right)\frac{\partial^2 u_z^0\left(x,y_{\mathrm{T}},z_{\mathrm{T}},t\right)}{\partial x^2} \tag{26}$$

$$M_z\left(x,y_{\mathrm{T}},z_{\mathrm{T}},t\right)\propto\left(-EI\right)\frac{\partial^2 u_y^0\left(x,y_{\mathrm{T}},z_{\mathrm{T}},t\right)}{\partial x^2} \tag{27}$$

$$V_y\left(x,y_{\mathrm{T}},z_{\mathrm{T}},t\right)\propto\left(-EI\right)\frac{\partial^3 u_y^0\left(x,y_{\mathrm{T}},z_{\mathrm{T}},t\right)}{\partial x^3} \tag{28}$$

$$V_z\left(x,y_{\mathrm{T}},z_{\mathrm{T}},t\right)\propto\left(-EI\right)\frac{\partial^3 u_z^0\left(x,y_{\mathrm{T}},z_{\mathrm{T}},t\right)}{\partial x^3} \tag{29}$$

Substituting Eq. (21) into Eqs. (25)–(29) in sequence results in:

$$\left|N_x\left(x,y_{\mathrm{T}},z_{\mathrm{T}},t\right)\right|_{\max}\propto\left|EA\frac{\partial u_x^0\left(x,y_{\mathrm{T}},z_{\mathrm{T}},t\right)}{\partial t}\right|_{\max} \tag{30}$$

$$\left|M_y\left(x,y_{\mathrm{T}},z_{\mathrm{T}},t\right)\right|_{\max}\propto\left|EI\frac{\partial^2 u_z^0\left(x,y_{\mathrm{T}},z_{\mathrm{T}},t\right)}{\partial t^2}\right|_{\max} \tag{31}$$

$$\left|M_z\left(x,y_{\mathrm{T}},z_{\mathrm{T}},t\right)\right|_{\max}\propto\left|EI\frac{\partial^2 u_y^0\left(x,y_{\mathrm{T}},z_{\mathrm{T}},t\right)}{\partial t^2}\right|_{\max} \tag{32}$$

$$\left|V_y\left(x,y_{\mathrm{T}},z_{\mathrm{T}},t\right)\right|_{\max}\propto\left|EI\frac{\partial^3 u_y^0\left(x,y_{\mathrm{T}},z_{\mathrm{T}},t\right)}{\partial t^3}\right|_{\max} \tag{33}$$

$$\left|V_z\left(x,y_{\mathrm{T}},z_{\mathrm{T}},t\right)\right|_{\max}\propto\left|EI\frac{\partial^3 u_z^0\left(x,y_{\mathrm{T}},z_{\mathrm{T}},t\right)}{\partial t^3}\right|_{\max} \tag{34}$$

Thus, the determinations of critical moments corresponding to the structural longitudinal seismic responses under obliquely incident in-plane waves are achieved. Similar to the derivation results of the SH wave incidence for an arbitrary point on the tunnel structure, the critical moments of its displacements and internal forces have relationships with relevant free-field movements. Once we obtain the free wave field, and afterward, its high-order derivatives with respect to the time variable t, it is convenient to determine the structural critical moments of longitudinal seismic responses under non-uniform earthquake excitations.

After confirming the critical moments of several physical quantities, a series of static calculations should be performed according to the remaining implementations of the proposed method. As a result, the maximal longitudinal seismic responses of the tunnel structure subjected to obliquely incident in-plane waves can be acquired.

5 Verification of the longitudinal integral response deformation method

To verify the precision and applicability of the proposed method, a series of longitudinal seismic response analyses of a tunnel structure under obliquely incident SH and SV waves is performed. Using the finite element software ABAQUS, the dynamic time-history method is conventionally employed as the technical standard.

5.1 Calculation object and parameters

A circular shield tunnel structure embedded at a depth of 15.0 m in the Beijing subway line is chosen as the research object. Two numerical models separately used for static and dynamic analyses have the same geometric dimensions that meet the demands of the specification (GB 50909-2014, China Planning Press, Beijing), i.e., a total length of 300.0 m in the longitudinal x-axis direction, a total width of 40.0 m in the horizontal y-axis direction, and a total height of 50.0 m in the vertical z-axis direction. The lining structure is composed of concrete flat-plate segments graded at C50, the inner and external diameters of which are 5.4 m and 6.0 m, respectively. Assuming the tunnel is embedded in the homogeneous soil layer, the mass density of the soil medium is 2000.0 kg/m^3 and the Poisson′s ratio is 0.3. The propagating velocity of shear waves is 300.0 m/s. Figure 5 illustrates the integral soil-tunnel finite element model. The soil medium and the underground tunnel are simulated by the use of solid elements and Timoshenko beam elements, respectively. When conducting the

Table 1 Ground motion records used for this study

Date	Earthquake	Station name	Component
01/16/1995	Kobe (M_w=6.90)	Kakogawa	East-West
10/18/1989	Loma Prieta (M_w=6.93)	Gilroy Array #3	East-West
01/17/1994	Northridge (M_w=6.69)	Castaic - Old Ridge Route	East-West

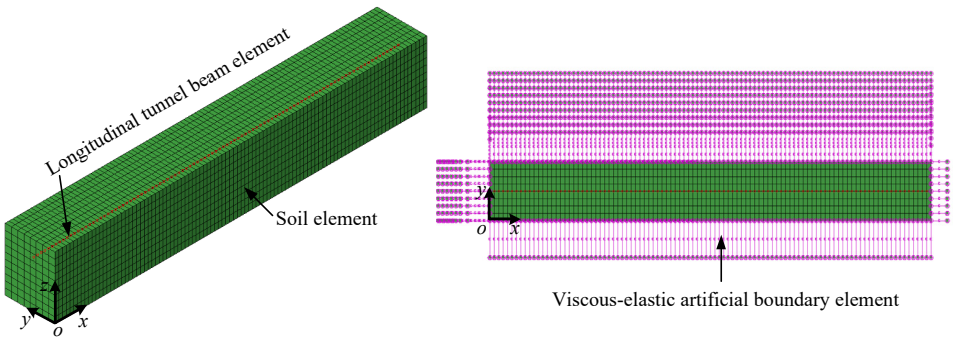

Fig. 5 Soil-tunnel finite element model

proposed method, fixed boundaries are established on all cutoff surfaces of the numerical model, which are replaced by the viscoelastic artificial boundaries (Liu *et al*., 2006) when using the dynamic time-history method. All the pink members in Fig. 5 represent the viscoelastic artificial boundary elements.

Three actual acceleration time histories, as recorded in the Kobe earthquake, the Loma Prieta earthquake and the Northridge earthquake, are considered as the input motions for this study, with a time duration of 40 s and a sampling time interval of 0.005 s. The source for these records is the Pacific Earthquake Engineering Research Center (PEER) strong motion database. Table 1 gives detailed information for each record. The amplitudes of input acceleration recordings are all scaled up to 0.1 g in the computing. In Fig. 6, the left part of each subfigure showed the input acceleration time history and the right part corresponds to a Fourier spectrum.

5.2 Seismic response analysis of the tunnel under obliquely incident SH waves

In this section, the longitudinal seismic response analysis of the tunnel under obliquely incident SH waves is performed using the proposed method and the dynamic time-history method. The incident angles of the SH waves are $\theta = 90°$, $\phi = 30°$ with the same definitions of θ, ϕ, as depicted in Fig. 3.

(1) Applying the proposed method

Following the abovementioned implementation procedure of the proposed method, the free wave field should be calculated first by using Eq. (1). Then, taking the midpoint of the tunnel as a reference (i.e., x=150.0 m), the critical moments corresponding to different physical quantities of the structural longitudinal seismic responses can be determined by using Eqs. (14)–(17). Subsequently, a series of free-field deformations at the

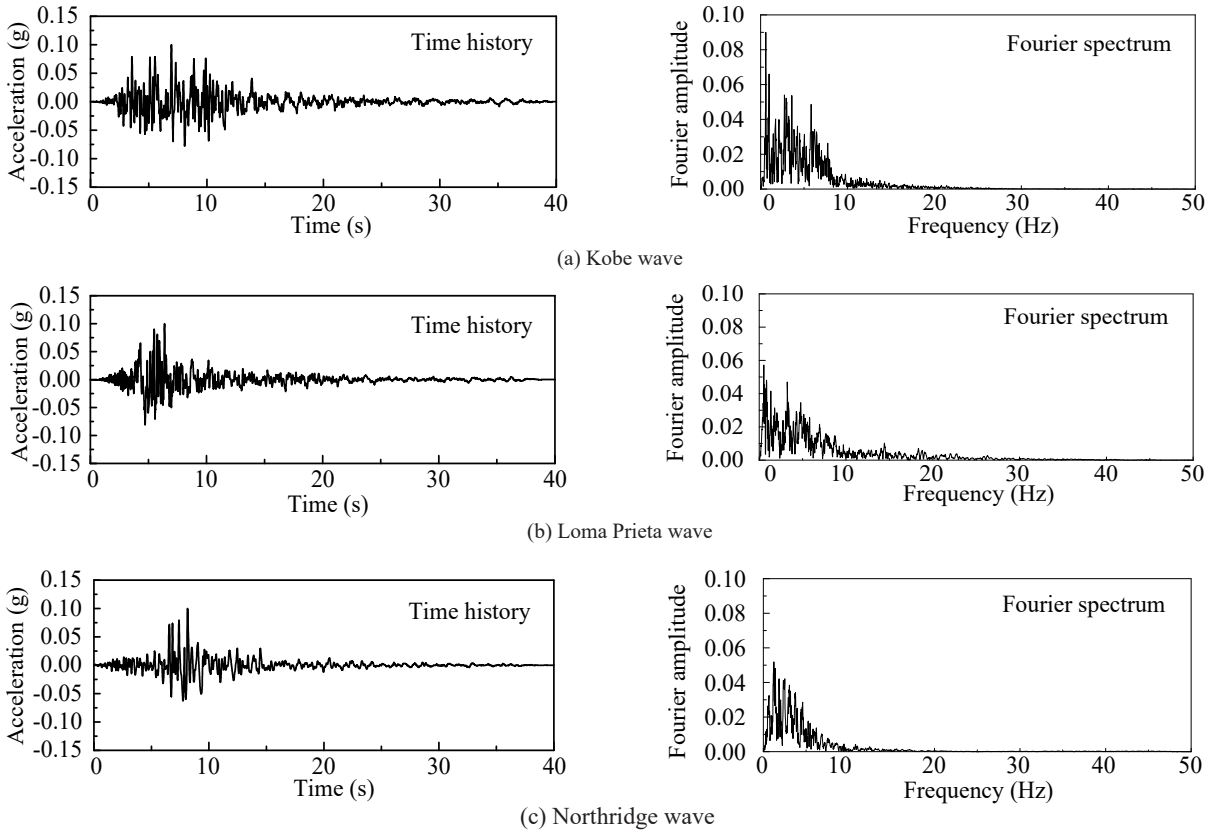

Fig. 6 Time history of the acceleration (left) and the Fourier amplitude of acceleration (right) of (a) Kobe wave; (b) Loma Prieta wave; (c) Northridge wave

Table 2 Calculation results of the proposed method under obliquely incident SH waves (θ = 90°, ϕ = 30°)

Seismic recording	u_{xs} (m)	u_{ys} (m)	N_{xs} (kN)	M_{zs} (kN·m)	V_{ys} (kN)
Kobe	–0.0266 (11.900 s)	0.0491 (11.900 s)	34608.07 (6.325 s)	–9041.62 (7.425 s)	–494.35 (10.335 s)
Loma Prieta	–0.0519 (5.265 s)	0.0938 (5.265 s)	55854.30 (4.845 s)	–8319.98 (6.860 s)	724.41 (6.010 s)
Northridge	0.0153 (7.320 s)	–0.0279 (7.320 s)	30391.66 (7.985 s)	–10007.46 (8.615 s)	–537.04 (8.550 s)

identified critical moments can be extracted; these are known as the least favorable free-field deformations. Due to the limited space available, only the least favorable free-field deformations under the obliquely incident Kobe wave are illustrated in Fig. 7.

According to the remaining calculation steps for the proposed method, the critical seismic responses of the tunnel in the longitudinal direction can be obtained after accomplishing relevant static computations. Table 2 lists the critical deformations (axial displacement u_{xs} and lateral displacement u_{ys}) and internal forces (axial force N_{xs}, bending moment M_{zs} and shear force V_{ys}) under different obliquely incident SH waves, as well as their relevant critical moments (shown in parentheses). Both Table 1 and Fig. 7 make it clear that the critical moments vary for different structural seismic responses. The least favorable free-field deformations are correspondingly diverse.

(2) Applying the dynamic time-history method

In the dynamic time-history analysis, the wave-motion method is employed to realize valid inputs of earthquake motions (Liu and Lv, 1998), which means the incident seismic wave is converted into the equivalent nodal loads acting on the viscoelastic

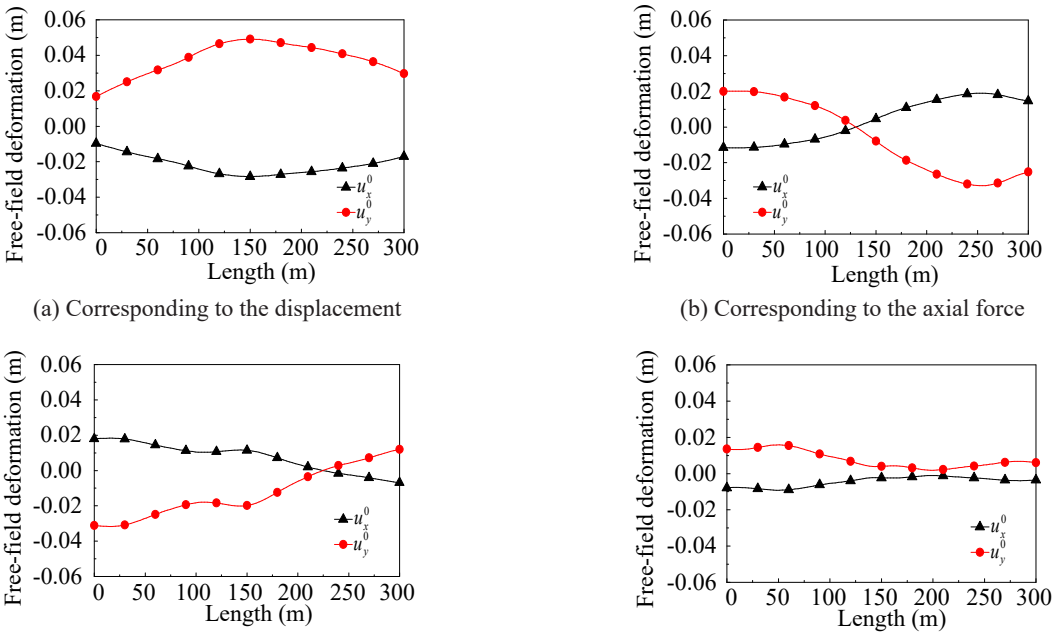

(a) Corresponding to the displacement

(b) Corresponding to the axial force

(c) Corresponding to the bending moment

(d) Corresponding to the shear force

Fig. 7 Least favorable free-field deformations under the obliquely incident Kobe wave ($\theta = 90°$, $\phi = 30°$)

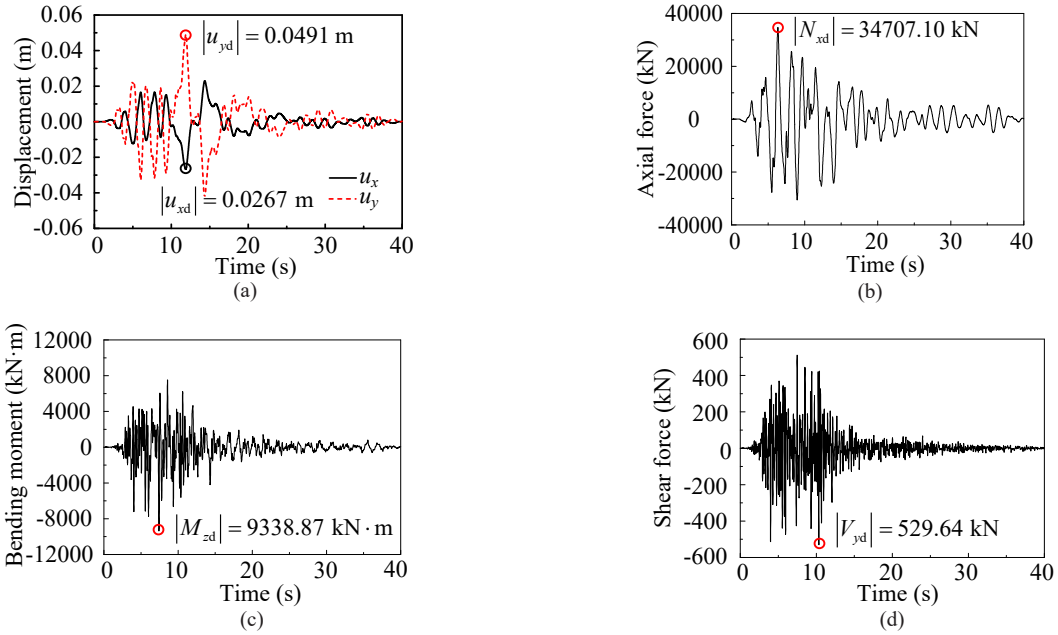

Fig. 8 Structural dynamic response under the Kobe input

artificial boundaries. The seismic response analysis of the three-dimensional soil-tunnel dynamic interaction system is conducted with assistance from the step-by-step time-integration method. The time-history curves of tunnel seismic responses for the obliquely incident Kobe wave are plotted in Fig. 8, for the Loma Prieta wave in Fig. 9 and for the Northridge wave in Fig. 10, including displacements u_x and u_y, axial force N_x, bending moment M_z and shear force V_y. By means of these time-history curves, the structural peak axial displacement u_{xd}, lateral displacement u_{yd}, axial force N_{xd}, bending moment M_{zd} and shear force V_{yd} can be extracted under different seismic recordings, as well as their respective peak moments. All of these results are presented in Table 3 and the values written in parentheses are the relevant peak moments.

(3) Comparison of the two methods

Table 4 summarizes the results of structural seismic responses as calculated by the proposed and dynamic time-history methods under different earthquake inputs and their relative errors. As seen in Table 3, the proposed method accurately predicts the amplitudes of structural displacements, including u_x and u_y under different seismic motions. Additionally, these data compare quite well with the data taken from the dynamic time-history method in terms of maximum internal forces. Specifically,

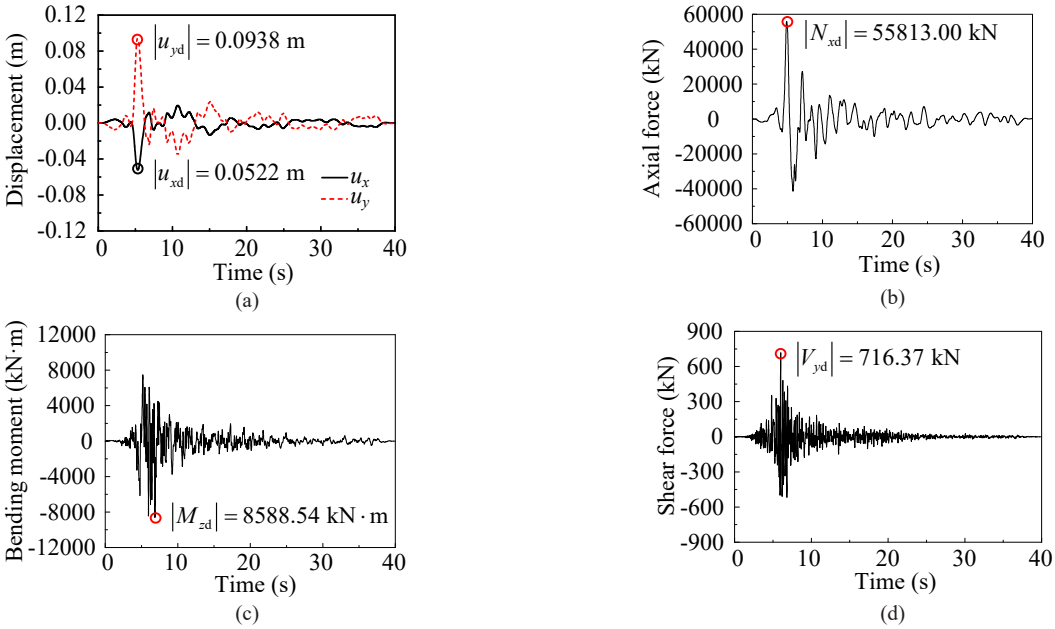

Fig. 9 Structural dynamic response under the Loma Prieta input

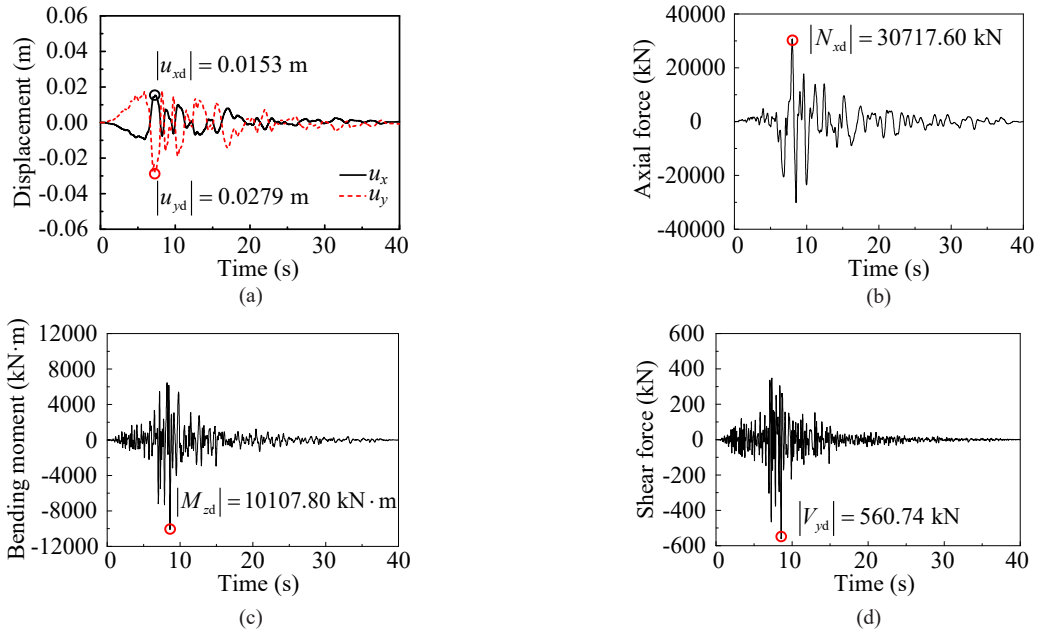

Fig. 10 Structural dynamic response under the Northridge input

the absolute maximum relative error is approximately 1% for the axial forces N_x, approximately 3% for the bending moments M_z, and less than 7% for the shearing forces V_y. In conclusion, the high compliance between the calculation results of the proposed method with the dynamic time-history analysis confirms the accuracy of the new method for the obliquely incident SH wave case. Meanwhile, this approach can dramatically lessen the calculation burden through static computations.

Table 5 presents the results of the critical moments t_s and the peak moments t_d, determined by the proposed method and the dynamic time-history analysis, respectively. It is observed that the critical moments t_s agree well with the peak moments t_d with a difference of no more than 0.05 s. Hence, instead of performing the complex dynamic time-history analysis of the three-dimensional integral soil-tunnel model, adopting the proposed method can properly and conveniently capture the critical moments corresponding to the least favorable longitudinal seismic responses of a tunnel structure.

5.3 Seismic response analysis of the tunnel under obliquely incident SV waves

To verify the effectiveness of the proposed method for oblique SV wave incidence, a series of numerical analyses are conducted herein under the same input acceleration recordings as used in the previous section, with incident angles of $\theta = 30°$, $\phi = 30°$. In the calculation model of this paper, since the Poisson′s ratio is 0.3 and the incident angle is $\theta = 30°$, which does not exceed the limit value of the SV wave, the free wave field contains the incident SV wave and the reflected SV and P waves from the free surface.

Table 3 Calculation results of the dynamic time-history method under obliquely incident SH waves (θ = 90º, ϕ = 30º)

Seismic recording	u_{xd} (m)	u_{yd} (m)	N_{xd} (kN)	M_{zd} (kN·m)	V_{yd} (kN)
Kobe	–0.0267	0.0491	34707.10	–9338.87	–529.64
	(11.875 s)	(11.900 s)	(6.340 s)	(7.425 s)	(10.330 s)
Loma Prieta	–0.0522	0.0938	55813.00	–8588.54	716.37
	(5.315 s)	(5.270 s)	(4.885 s)	(6.860 s)	(6.005 s)
Northridge	0.0153	–0.0279	30717.60	–10107.80	–560.74
	(7.345 s)	(7.325 s)	(7.995 s)	(8.625 s)	(8.565 s)

Table 4 Comparison of the calculation results under obliquely incident SH waves (θ = 90º, ϕ = 30º)

Seismic recording	Calculation method	Longitudinal seismic responses of the tunnel structure				
		u_x (m)	u_y (m)	N_x (kN)	M_z (kN·m)	V_y (kN)
Kobe	Proposed	–0.0266	0.0491	34608.07	–9041.62	–494.35
	Dynamic	–0.0267	0.0491	34707.10	–9338.87	–529.64
	Relative error	–0.37%	0	–0.29%	–3.18%	–6.66%
Loma Prieta	Proposed	–0.0519	0.0938	55854.30	–8319.98	724.41
	Dynamic	–0.0522	0.0938	55813.00	–8588.54	716.37
	Relative error	–0.57%	0	0.07%	–3.13%	1.12%
Northridge	Proposed	0.0153	–0.0279	30391.66	–10007.46	–537.04
	Dynamic	0.0153	–0.0279	30717.60	–10107.80	–560.74
	Relative error	0	0	–1.06%	–0.99%	–4.23%

Table 5 Comparison of the critical moments under obliquely incident SH waves (θ = 90º, ϕ = 30º)

Seismic recording		Critical moments corresponding to the structural seismic responses				
		u_x	u_y	N_x	M_z	V_y
Kobe	t_s (s)	11.900	11.900	6.325	7.425	10.335
	t_d (s)	11.875	11.900	6.340	7.425	10.330
Loma Prieta	t_s (s)	5.265	5.265	4.845	6.860	6.010
	t_d (s)	5.315	5.270	4.885	6.860	6.005
Northridge	t_s (s)	7.320	7.320	7.985	8.615	8.550
	t_d (s)	7.345	7.325	7.995	8.625	8.550

(1) Applying the proposed method

The free wave field under obliquely incident SV waves can be calculated as in Eq. (18). Still taking the midpoint of the tunnel as a reference (i.e., x=150.0 m), a set of critical moments can be determined by Eqs. (30)–(34).

Figure 11 only demonstrates the least favorable free-field deformations under the obliquely incident Kobe wave in view of the limited space.

Table 6 illustrates the calculation results of the proposed method under different obliquely incident SV waves, including critical displacements (axial displacement u_{xs}, lateral displacement u_{ys} and vertical displacement u_{zs}) and internal forces (axial force N_{xs}, bending moments M_{ys} and M_{zs} around the y-axis and the z-axis, respectively), as well as their relevant critical moments (listed in parentheses). It should be stressed that the values of shear forces are not presented in the following calculation results, due to their relatively small magnitudes.

(2) Applying the dynamic time-history method

The time-history curves of the tunnel seismic responses for the obliquely incident Kobe waves are plotted in Fig. 12, for the Loma Prieta wave in Fig. 13, and for the Northridge wave in Fig. 14, including displacements u_x, u_y and u_z, the axial forces N_x, and bending moments M_y and M_z. By means of these time-history curves, the structural peak axial displacement u_{xd}, the lateral displacement u_{yd}, the vertical displacement u_{zd}, the axial force N_{xd}, the bending moment around the y-axis M_{yd}, and the bending moment around the z-axis M_{zd} can be separately extracted, as well as their respective peak moments. All of these results are listed in Table 7, and the values written in parentheses represent the relevant peak moments.

(3) Comparison of the two methods

For the case of obliquely incident SV waves, the results of structural seismic responses by the use of the proposed and dynamic time-history methods under different earthquake inputs are tabulated in Table 8, along with their relative errors. It can be seen that the proposed method produces good agreement with the maximum structural deformations, including the components u_x, u_y and u_z. It also compares quite well with the dynamic time-history method in terms of

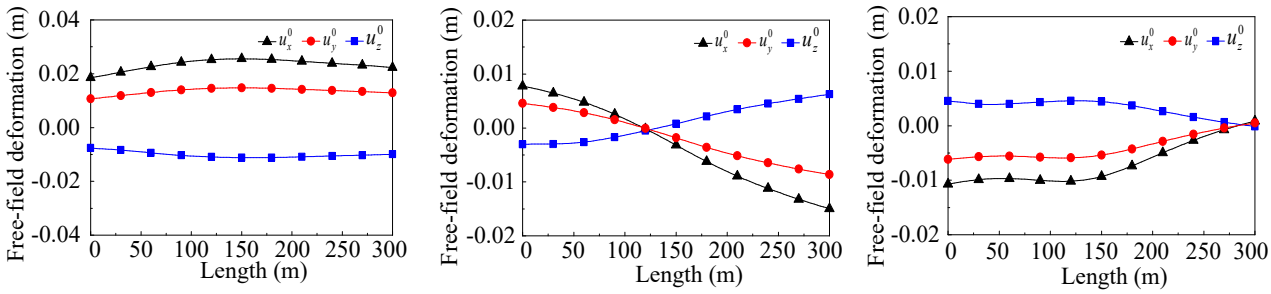

(a) Corresponding to the displacement (b) Corresponding to the axial force (c) Corresponding to the bending moment

Fig. 11 Least favorable free-field deformations under the obliquely incident Kobe wave (θ = 90°, ϕ = 30°)

Table 6 Calculation results of the proposed method under obliquely incident SV waves (θ = 30°, ϕ = 30°)

Seismic recording	u_{xs} (m)	u_{ys} (m)	u_{zs} (m)	N_{xs} (kN)	M_{ys} (kN·m)	M_{zs} (kN·m)
Kobe	0.0251 (11.800 s)	0.0147 (11.800 s)	–0.0112 (11.800 s)	–17468.50 (6.240 s)	497.56 (7.300 s)	–596.82 (7.300 s)
Loma Prieta	0.0486 (5.180 s)	0.0283 (5.180 s)	-0.0215 (5.180 s)	–26989.90 (4.760 s)	513.12 (6.750 s)	–522.28 (6.750 s)
Northridge	–0.0142 (7.235 s)	–0.0084 (7.235 s)	0.0064 (7.235 s)	16607.57 (8.445 s)	570.62 (8.500 s)	–680.91 (8.500 s)

Table 7 Calculation results of the dynamic time-history method under obliquely incident SV waves (θ = 30°, ϕ = 30°)

Seismic recording	u_{xd} (m)	u_{yd} (m)	u_{zd} (m)	N_{xd} (kN)	M_{yd} (kN·m)	M_{zd} (kN·m)
Kobe	0.0251 (11.790 s)	0.0147 (11.790 s)	–0.0112 (11.790 s)	–17465.90 (6.235 s)	494.55 (7.310 s)	–601.74 (7.325 s)
Loma Prieta	0.0486 (5.205 s)	0.0283 (5.205 s)	–0.0214 (5.205 s)	–26701.70 (4.770 s)	546.26 (6.755 s)	–545.95 (6.765 s)
Northridge	–0.0142 (7.240 s)	–0.0084 (7.240 s)	0.0064 (7.240 s)	16873.10 (8.430 s)	595.34 (8.500 s)	–683.05 (8.530 s)

maximum internal forces. To be specific, the absolute maximum relative error of the axial force N_x is less than 2%, the bending moment around the y-axis M_y is approximately 6%, and the bending moment around the z-axis M_z is approximately 4%. In conclusion, the high degree of compliance between the calculation results of the proposed method and the dynamic time-history analysis confirms the accuracy of the new method for the obliquely incident SV waves.

Table 9 presents the comparison between the critical moment t_s of the proposed method and the peak moment t_d of the dynamic time-history analysis. It is observed that the critical moments agree well with the peak moments with absolute relative errors of no more than 0.5%. Hence, instead of performing the complex dynamic time-history analysis, adopting the proposed method can properly and conveniently capture the critical moments corresponding to the least favorable longitudinal seismic responses of a tunnel structure under SV waves.

5.4 Comparison of computational efficiency of different methods

There are four key aspects in the longitudinal seismic response analysis of the tunnel structure: (1) determination of the free wave field; (2) processing of

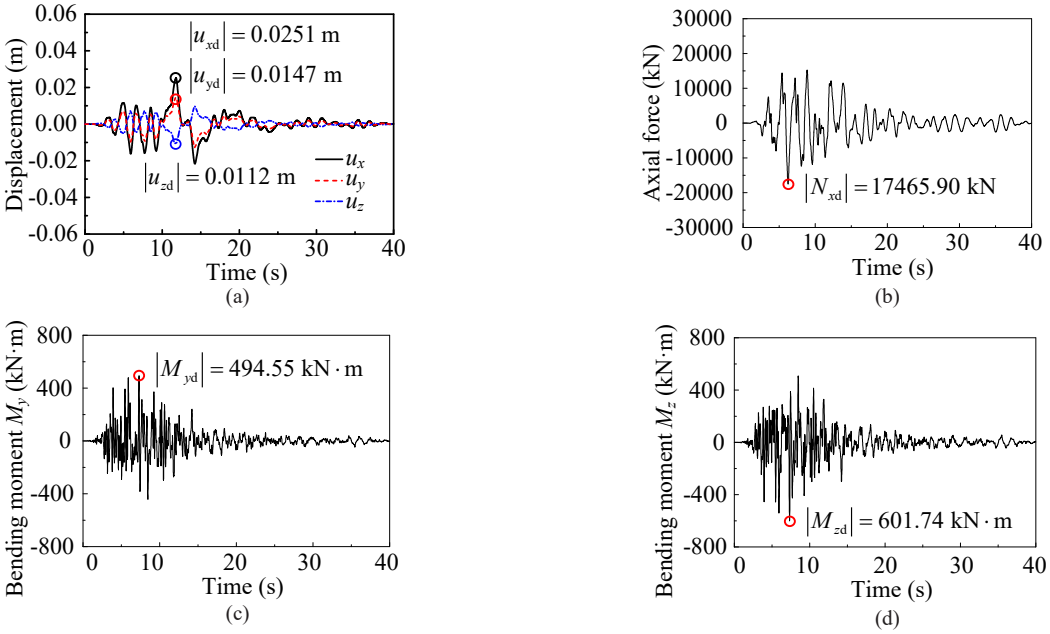

Fig. 12 Structural dynamic response under the Kobe input

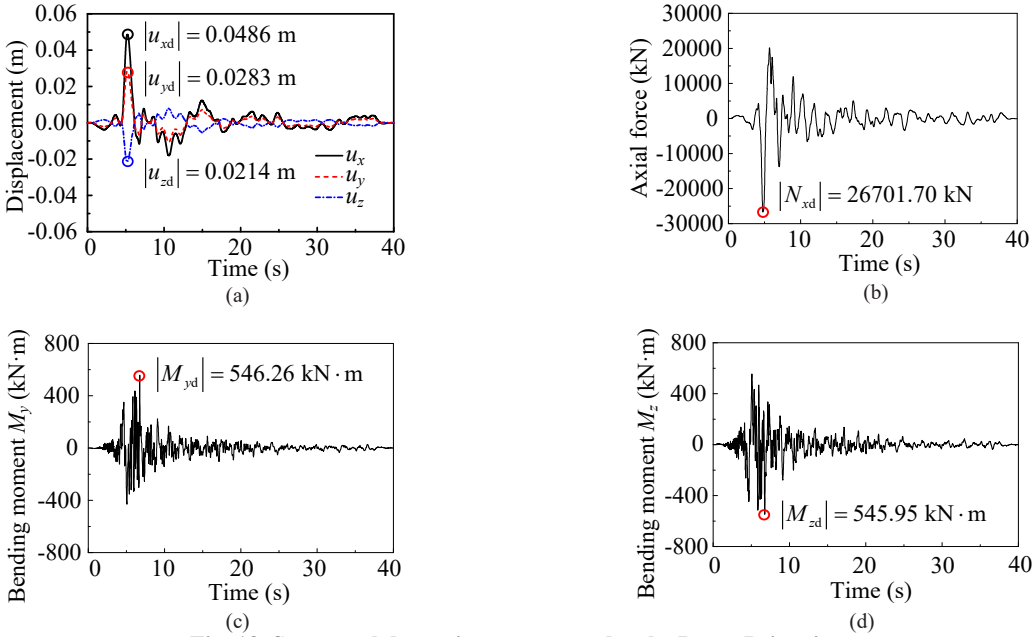

Fig. 13 Structural dynamic response under the Loma Prieta input

the artificial boundary condition; (3) seismic wave input; and (4) calculation of the foundation-tunnel structure seismic response. Since the dynamic time-history method and the proposed method both have basically the same calculation process when solving the free-field seismic response, these two methods are compared from the other three aspects to illustrate that the proposed method has higher computational efficiency, as in the following discussion.

(1) Processing of the artificial boundary condition

In the dynamic time-history analysis, artificial boundaries (such as viscous boundaries, viscous-elastic boundaries, etc.) are generally set on truncation surfaces, which are the bottom surface and the four sides of the analysis model. In this study, the viscous-elastic boundaries are adopted. Specifically, the parallel spring-damper units are respectively arranged in the normal direction and the tangential direction of each node of the artificial boundary.

The proposed method in this paper belongs to the static analysis method, and the fixed boundary conditions are established on the artificial boundary surfaces.

Fixed boundary conditions are much simpler than viscous or viscous-elastic boundaries.

(2) Seismic wave input

In order to achieve seismic wave input, both analytical methods need to determine the equivalent seismic load.

In the dynamic time-history analysis, the equivalent seismic load is the dynamic action that varies with space and time. That is, for each artificial boundary node, the equivalent load is simultaneously different and a time function. It should be applied to the bottom surface and four sides of the analysis model.

The equivalent seismic load of the proposed method is static. It is calculated by the free-field displacement corresponding to the tunnel location at different critical moments. The equivalent seismic load is applied to the

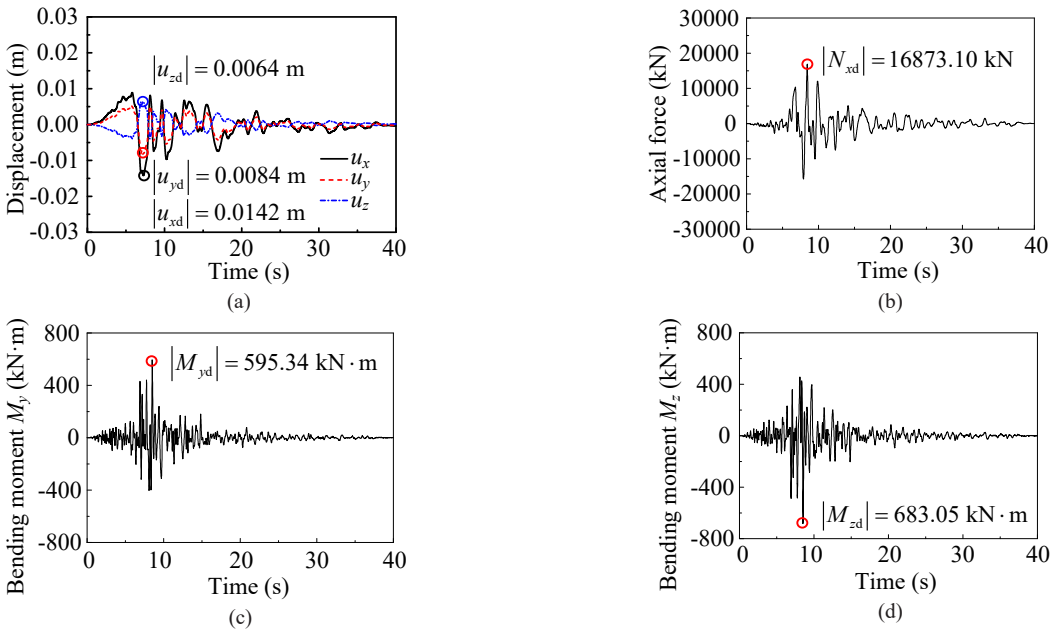

Fig. 14 Structural dynamic response under the Northridge input

Table 8 Comparison of the calculation results under obliquely incident SV waves ($\theta = 30°$, $\phi = 30°$)

Seismic recording	Calculation method	Longitudinal seismic responses of the tunnel structure					
		u_x (m)	u_y (m)	u_z (m)	N_x (kN)	M_y (kN·m)	M_z (kN·m)
Kobe	Proposed	0.0251	0.0147	–0.0112	–17468.50	497.56	–596.82
	Dynamic	0.0251	0.0147	–0.0112	–17465.90	494.55	–601.74
	Relative error	0	0	0	0.01%	0.61%	–0.82%
Loma Prieta	Proposed	0.0486	0.0283	–0.0215	–26989.90	513.12	–522.28
	Dynamic	0.0486	0.0283	–0.0214	–26701.70	546.26	–545.95
	Relative error	0	0	0.47%	1.08%	–6.07%	–4.34%
Northridge	Proposed	–0.0142	–0.0084	0.0064	16607.57	570.62	–680.91
	Dynamic	–0.0142	–0.0084	0.0064	16873.10	595.34	–683.05
	Relative error	0	0	0	–1.57%	–4.15%	–0.31%

Table 9 Comparison of the critical moments under obliquely incident SV waves ($\theta = 30^o$, $\phi = 30^o$)

Seismic recording	Critical moments corresponding to structural seismic responses				
		u	N_x	M_y	M_z
Kobe	t_s (s)	11.800	6.240	7.300	7.300
	t_d (s)	11.790	6.235	7.310	7.325
Loma Prieta	t_s (s)	5.180	4.760	6.750	6.750
	t_d (s)	5.205	4.770	6.755	6.765
Northridge	t_s (s)	7.235	8.445	8.500	8.500
	t_d (s)	7.240	8.430	8.500	8.530

Table 10 Computing time of different methods

Analysis method	Boundary condition	Domain of seismic input	Computing time (s)
Dynamic method	Viscous-elastic artificial boundaries	Bottom surface and four sides of the soil-tunnel integral finite element model	7915
Proposed method	Fixed boundaries	The wire-frame beam model	136

Note: The computing time of the proposed method listed in Table 10 is the total time required to solve the displacements and internal forces of the tunnel structure.

beam element, which is built to simulate the tunnel structure, rather than the five truncation surfaces of the analysis model.

The calculation and application of static loads are much simpler and more convenient than dynamic loads.

(3) Calculation of the foundation-tunnel structure seismic response

The workstation used in this study is the Lenovo ThinkStation P910, with a CPU of Intel Xeon E5-2637 v4 @ 3.50GHz and RAM of 96 GB. Table 10 shows the computing time of the dynamic time-history analysis method and the proposed method. It can be seen that the computing time of the proposed method is only 1.7% of the dynamic method.

6 Conclusions

In this paper a new type of integral response deformation method is proposed, one that is applicable to the longitudinal aseismic analysis of tunnel structures. When applying the proposed method, equivalent seismic loads imposing on the interface between the tunnel and foundation can be acquired through a static analysis of the relevant free-field model. The critical seismic responses of the tunnel structure can be obtained by completing the static calculation of the integral tunnel-foundation model. Different numerical examples show that the proposed method has a well-defined physical concept and high computational precision. Compared to the dynamic time-history method, the proposed method is more time saving, with a simpler process and less computational effort. This method can be used for an aseismic analysis of long-line underground tunnels that are subjected to asynchronous earthquake inputs.

An approach to define the critical moments of the structural deformations and the internal forces is also put forward in this paper. Theoretically, it is necessary to determine the varying laws of spatial waveforms in three-dimensional fields to determinate critical moments. However, the proposed approach simplifies the issue into that of analyzing how the motion time-history of a point in the elastic space changes over time. This approach is especially convenient for distinguishing critical moments when dealing with actual earthquake records.

According to the calculation procedure and analysis model discussed above, the proposed method can be applied to work out the critical responses of underground tunnel structures due to different forms of seismic waves. The dynamic interaction between the structure and the soil medium is counted directly, thereby avoiding the computational error caused by discrete foundation springs.

Specifically, the finite element model of the soil medium is assumed to be linearly elastic without considering the nonlinearity of the soil material discussed in this paper. This is because it is complicated and requires significant effort to accomplish the nonlinear seismic analysis of soil layers in three dimensions due to the oblique incidence of seismic wave. In this regard, some equivalent-linear methods for analyzing seismic responses of soil layers in geotechnical engineering could be used for reference (Qi and Bo, 2007; Wang and Zhao, 2016).

Notably, although the underground tunnel is simplified into a beam model to clarify the application and verification of the method put forward in this paper, the proposed method has no limit on the geometric shape or dimension of the analyzed tunnel. Therefore, the longitudinal integral response deformation method

is encouraged to analyze the seismic responses of underground structures with large-scale or variable cross sections.

References

Bardet JP, Ichii K and Lin CH (2000), "EERA: A Computer Program for Equivalent-Linear Earthquake Site Response Analyses of Layered Soil Deposits," University of Southern California, Los Angeles.

Fu Jia, Liang Jianwen and Qin Lin (2016), "Dynamic Soil-Tunnel Interaction in Layered Half-Space for Incident Plane SH Waves," *Earthquake Engineering and Engineering Vibration*, **15**(4): 715–727.

GB 50267-97 (1998), *Code for Seismic Design of Nuclear Power Plants*, Ministry of Housing and Urban-Rural Development of the People′s Republic of China, China Planning Press, Beijing. (in Chinese)

GB 50909-2014 (2014), *Code for Seismic Design of Urban Rail Transit Structures*, Ministry of Housing and Urban-Rural Development of the People′s Republic of China, China Planning Press, Beijing. (in Chinese)

Gu Yin, Chen Kai, Wu Huaiqiang, Zhuo Weidong and Sun Ying (2017), "Shaking Table Tests for a Subway Station Structure Under Spatially Non-Uniform Ground Motion," *Journal of Vibration and Shock*, **36**(17): 256–261. (in Chinese)

He Chuan, Zhang Jing, and Feng Kun (2017), "Research on Structural Analysis Method of Shield Tunnels," *China Journal of Highway and Transport*, **30**(8): 1–14. (in Chinese)

Idriss IM and Sun JI (1992), "User′s Manual for SHAKE91," *Center for Geotechnical Modeling*, **388**(5-6): 279–360.

Jiang Luzhen, Chen Jun and Li Jie (2010), "Seismic Response of Underground Utility Tunnels: Shaking Table Testing and FEM Analysis," *Earthquake Engineering and Engineering Vibration*, **9**(4): 555–567.

John CMS and Zahrah TF (1987), "Aseismic Design of Underground Structures," *Tunnelling & Underground Space Technology Incorporating Trenchless Technology Research*, **2**(2): 165–197.

Knopoff L (1964), "A Matrix Method of Elastic Wave Problems," *Bulletin of the Seismological Society of America*, **54**(1): 431–438.

Li Liyun, Wang Chengbo, Han Junyan, Hou Benwei, Xu Chengshun and Du Xiuli (2015), "Analysis of Site Responses During Shaking Table Test for the Interaction between Pipeline and Soil," *Earthquake Engineering and Engineering Dynamics*, **35**(3): 166–176. (in Chinese)

Li Peng (2013), "Numerical Analysis for Longitudinal Seismic Response of Tunnels in Saturated Soil," Tsinghua University, Beijing. (in Chinese)

Liu Jingbo, Du Yixin, Du Xiuli, Wang Zhenyu and Wu Jun (2006), "3D Viscous-Spring Artificial Boundary in Time Domain," *Earthquake Engineering and Engineering Vibration*, **5**(1): 93–102.

Liu Jingbo and Lv Yandong (1998), "A Direct Method for Analysis of Dynamic Soil-Structure Interaction," *China Civil Engineering Journal*, **31**(3): 55–64. (in Chinese)

Liu Jingbo, Wang Wenhui and Dasgupta Gautam (2014), "Pushover Analysis of Underground Structures: Method and Application," *Science China: Technological Sciences*, **57**(2): 423–437.

Liu Jingbo, Wang Wenhui and Zhao Dongdong (2013a), "Comparison of the Pseudo-Static Methods for Seismic Analysis of the Underground Structures," *Engineering Mechanics*, **30**(1): 105–111. (in Chinese)

Liu Jingbo, Wang Wenhui, Zhao Dongdong and Zhang Xiaobo (2013b), "Integral Response Deformation Method for Seismic Analysis of Underground Structure," *Chinese Journal of Rock Mechanics and Engineering*, **32**(8): 1618–1624.

Liu Jingbo, Wang Wenhui, Zhao Dongdong and Zhang Xiaobo (2014), "Integral Response Deformation Method in Seismic Analysis of Complex Section Underground Structures," *Chinese Civil Engineering Journal*, **47**(1): 134–142.

Liu Jingbo and Wang Yan (2006), "A 1-D Time-Domain Method for 2D Wave Motion in Elastic Half-Spaced by Anti-Plane Wave Oblique Incidence," *China Journal of Theoretical and Applied Mechanics*, **38**(2): 219–225. (in Chinese)

Liu Jingbo and Wang Yan (2007), "A 1-D Time-Domain Method for In-Plane Wave Motion of Free-Field in Layered Media," *Engineering Mechanics*, **24**(7): 16–22. (in Chinese)

Liu Rushan and Shi Hongbin (2006), "An Improved Pseudo-Static Method for Seismic Resistant Design of Underground Structures," *Earthquake Engineering and Engineering Vibration*, **5**(2): 189–193.

Qi Wenhao and Bo Jingshan (2007), "Summarization on Equivalent Linear Method of Seismic Responses for Soil Layers," *World Earthquake Engineering*, **23**(4): 223–228. (in Chinese)

Shao Runmeng and Lei Yang (2013), "Longitudinal Anti-Seismic Analysis of Shield Tunnel Based on Response Deformation Method," *China Civil Engineering Journal*, **46**(S2): 260–265. (in Chinese)

Tateishi A (2005), "A Study on Seismic Analysis Methods in the Cross Section of Underground Structures Using Static Finite Element Method," *Structural Engineering*, **22**(1): 41–54.

Wang Duguo and Zhao Chenggang (2016), "Two-Dimensional Equivalent Linear Seismic Analysis of Free Field in Layered Half-space Due to Oblique Incidence," *Chinese Journal of Geotechnical Engineering*, **38**(3): 554–561. (in Chinese)

Wolf JP and Obernhuber P (1982a), " Free-Field

Response from Inclined SH-Waves and Love-Waves," *Earthquake Engineering and Structural Dynamics*, **10**(6): 823–845.

Wolf JP and Obernhuber P (1982b), "Free-Field Response from Inclined SV- and P-Waves and Rayleigh-Waves," *Earthquake Engineering and Structural Dynamics*, **10**(6): 847–869.

Xu Chengshun, Xu Zigang, Du Xiuli and Li Yang (2017), "Comparative Study of Simplified Methods for Seismic Analysis of Underground Structure," *Earthquake Engineering and Engineering Dynamics*, **37**(2): 65–80.

Yu Haitao, Yan Xiao, Antonio Bobet, Yuan Yong, Xu Guoping and Su Quanke (2018), "Multi-Point Shaking Table Test of a Long Tunnel Subjected to Non-Uniform Seismic Loadings," *Bulletin of Earthquake Engineering*, **16**(2): 1041–1059.

Zhao Mi, Du Xiuli, Liu Jingbo and Han Qiang (2013), "Time-Domain Method for Free Field in Layered Half Space under P-SV Waves of Oblique Incidence," *China Earthquake Engineering Journal*, **35**(1): 84–90. (in Chinese)